energies

MDPI

Article

Experimental Investigation of the Heat Transfer between Finned Tubes and a Bubbling Fluidized Bed with Horizontal Sand Mass Flow

Stefan Thanheiser *, Markus Haider and Paul Schwarzmayr

Institute for Energy Systems and Thermodynamics, TU Wien, 1040 Vienna, Austria; markus.haider@tuwien.ac.at (M.H.); paul.schwarzmayr@tuwien.ac.at (P.S.)
* Correspondence: stefan.thanheiser@tuwien.ac.at; Tel.: +43-1-58801-302-326

Abstract: The sandTES technology utilizes a fluidized bed counter current heat exchanger for thermal energy storage applications. Its main feature is an imposed horizontal flow of sand (SiO_2) particles fluidized by a vertical air flow across a heat exchanger consisting of several horizontal rows of tubes. Past international research on heat transfer in dense fluidized beds has focused on stationary (stirred tank) systems, and there is little to no information available on the impact of longitudinal or helical fins. Previous pilot plant scale experiments at TU Wien led to the conclusion that the currently available correlations for predicting the heat transfer coefficient between the tube surface and the surrounding fluidized bed are insufficient for the horizontal sand flow imposed by the sandTES technology. Therefore, several smaller test rigs were designed in this study to investigate the influence of different tube arrangements and flow conditions on the external convective heat transfer coefficient and possible improvements by using finned tubes. It could be shown that helically finned tubes in a transversal arrangement, where the horizontal sand flow is perpendicular to the tube axes, allows an increase in the heat transfer coefficient per tube length (i.e., the *virtual* heat transfer coefficient) by a factor of 3.5 to about 1250 W/m^2K at ambient temperature. Based on the literature, this heat transfer coefficient is expected to increase at higher temperatures. The new design criteria allow the design of compact, low-cost heat exchangers for thermal energy storage applications, in particular electro-thermal energy storage.

Keywords: bubbling fluidized bed; fluidized bed heat exchanger; heat transfer; finned tubes; horizontal tubes; sandTES; thermal energy storage; electro-thermal energy storage

Citation: Thanheiser, S.; Haider, M.; Schwarzmayr, P. Experimental Investigation of the Heat Transfer between Finned Tubes and a Bubbling Fluidized Bed with Horizontal Sand Mass Flow. *Energies* **2022**, *15*, 1316. https://doi.org/10.3390/en15041316

Academic Editor: Ahmed Elatar

Received: 23 December 2021
Accepted: 8 February 2022
Published: 11 February 2022

1. Introduction

The sandTES technology developed at TU Wien in Austria utilizes pressure gradients to impose a horizontal sand mass flow in a fluidized bed, pictured in Figure 1.

This system can be used to have the sand flow in the opposite direction of a heat transfer fluid (HTF) inside an immersed tube bundle to create a counter-current heat ex-changer, envisioned for thermal energy storage (TES) applications.

The sizing of such a heat exchanger requires accurate predictions of the heat transfer behavior between the tubes and the surrounding fluidized bed. Many experimental investigations have been published and several semi-empirical calculation methods have been developed for this purpose.

Chen [1] (pp. 261–266) arranges these correlations into four categories, the gaseous boundary layer approach (e.g., Andeen and Glicksman [2], Bansal [3] or Grewal [4]); the combined gaseous and particle convection model (e.g., Molerus [5]); the so-called packet theory model (Mickley and Fairbanks [6]); and finally, the kinetic motion analogy model by Martin [7].

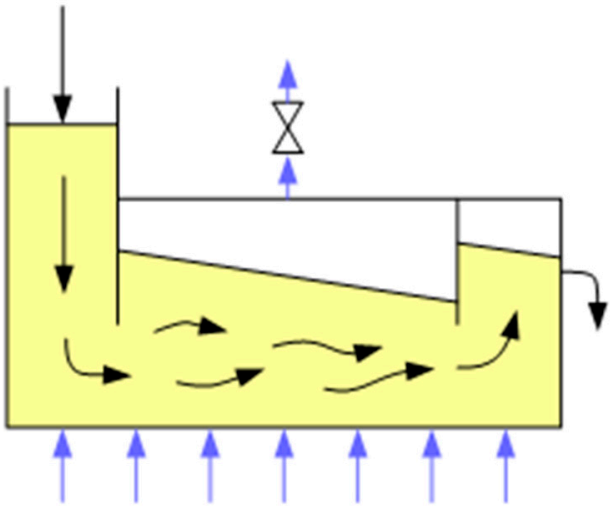

Figure 1. Sketch of the sandTES fluidized bed heat exchanger. Black arrows represent the flow of sand (yellow), while blue arrows show the fluidization air flow. The valve at the top is used to create a pressure zone (so-called air cushion) to control the sand level below. Both sand and fluidization gas are external flows.

Kunii and Levenspiel [8] (pp. 323–329) developed a generalized model that includes Mickley and Fairbank's packet theory model for the particle convective heat transfer. More recent investigations were conducted by Natale [9], Kim [10] and Pisters [11].

Some of the correlations mentioned above describe the heat transfer on any kind of surface, such as Mickley and Fairbanks, while others consider tubes as the heat transfer area, such as Andeen/Glicksman and Molerus. Only some include the effect of staggered tubes in a bundle, such as Grewal.

An overall conclusion is that there is no generally accepted and undisputed correlation that would allow the proper sizing of a heat exchanger in a fluidized bed. Additionally, none of these authors investigated the influence of a horizontal share in the sand mass flow or the effect of finned tubes.

A sandTES pilot plant with a mean particle diameter of 87 µm, plain tube diameter of 25 mm and operating in a temperature range of 20 °C to 400 °C was designed in 2014 [12–14]. Applying all the different correlations reported by Chen, including Kunii/Levenspiel and Martin, yields a range of the predicted heat transfer coefficient (HTC) between 250 and 600 W/m^2K in this case. This high uncertainty for a horizontal plain tube bundle does not even account for the influence of particle crossflow, tube bundle geometry, or the influence of fins. Additionally, the influence of particle diameter is considered differently in practically all correlations.

Since the achievable HTC is critical to the marketability of the entire sandTES technology, it was decided to conduct small scale experiments to determine the optimal tube bundle configuration and particle size to maximize the HTC. For this purpose, three test rigs were designed, of which a simplified sketch can be seen in Figure 2.

Electrically heated tubes were used to focus on the outer HTC between the tube surface and the fluidized bed. The three different test rigs are:

- MICRO: A single-cell model for stirred tank experiments. This means that, even though a small sand mass flow was circulating through this test rig, it did not have an established flow direction and was small enough that it could be ignored. This test rig served to analyze the performance of the utilized tube spacing in the sandTES plant compared to regular tube spacing. Previous simulations suggested that a narrower tube spacing would force fluidization onto a less regular path and thereby reduce poorly fluidized zones in the bed between the tubes, which would improve heat

transfer behavior [12] (pp. 162–163, 170). Additionally, this test rig was used to compare the performance of the 87 µm sand to coarser sand.

- LINI: (Longitudinal mINIature) This test rig simulated sand flow in parallel to the axes of the heat exchanger tubes, which were the conditions in the sandTES pilot plant. In addition, longitudinal fins for performance enhancement were investigated in this test rig.
- TRINI: (Transversal mINIature) Used to simulate sand flow perpendicular to the axes of the immersed heat exchanger tube bundle. This configuration offers several design advantages over longitudinal tubes while establishing greater impediment to sand flow. Helical fins were also investigated. The hatched plane in Figure 2 demonstrates that the influence of a baffle introduced between the tubes was investigated as well (refer to Section 2.1).

Helically finned tubes with transversal sand flow proved to be far superior to all other configurations. In addition, the better performance of the tube spacing of the sandTES pilot plant was verified.

Section 2 describes the design of the different test rigs and the measurement principles used. Section 3 presents and the results of the experiments which are then discussed and analyzed in Section 4.

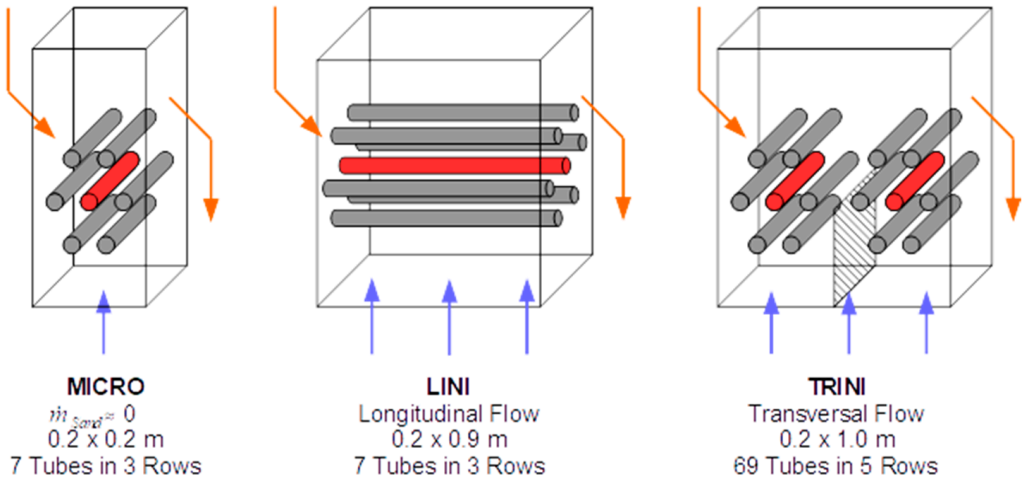

Figure 2. Schematic of the different test rigs used. Orange lines denote sand flow and blue lines indicate air flow. Red tubes are electrically heated, while gray tubes are dummy tubes introduced to establish the flow conditions around a bundle of tubes.

2. Materials and Methods

2.1. Test Rig Setup and Configuration

A generalized sketch of the three test rigs (MICRO, LINI, and TRINI) is shown in Figure 3. The different configurations of heat exchanger tube bundles were immersed in a fluidized bed. The bed material was quartz sand (SiO_2) and was fluidized using pressurized dry air, which was supplied by a compressor and subsequently dried to a dew point of 3 °C at 10 barg. The fluidization gas went through a porous (sintered) plate in all test rigs to ensure an even distribution and was always around or slightly above ambient temperature (~20 °C) in all experiments (see raw data for details). The sand was supplied on one side of the rig into a vertical tube whose bottom opening was dipped into the fluidized bed below. The sand level inside the tube then created a hydrostatic pressure that forced the sand to flow horizontally across the electrically heated tube bundle to the other side, where a pneumatic transport system conveyed it back again while also cooling the heated sand down. This resulted in a bed temperature of around 40 °C when operating the test rigs in a stationary state and a sand supply temperature slightly below that.

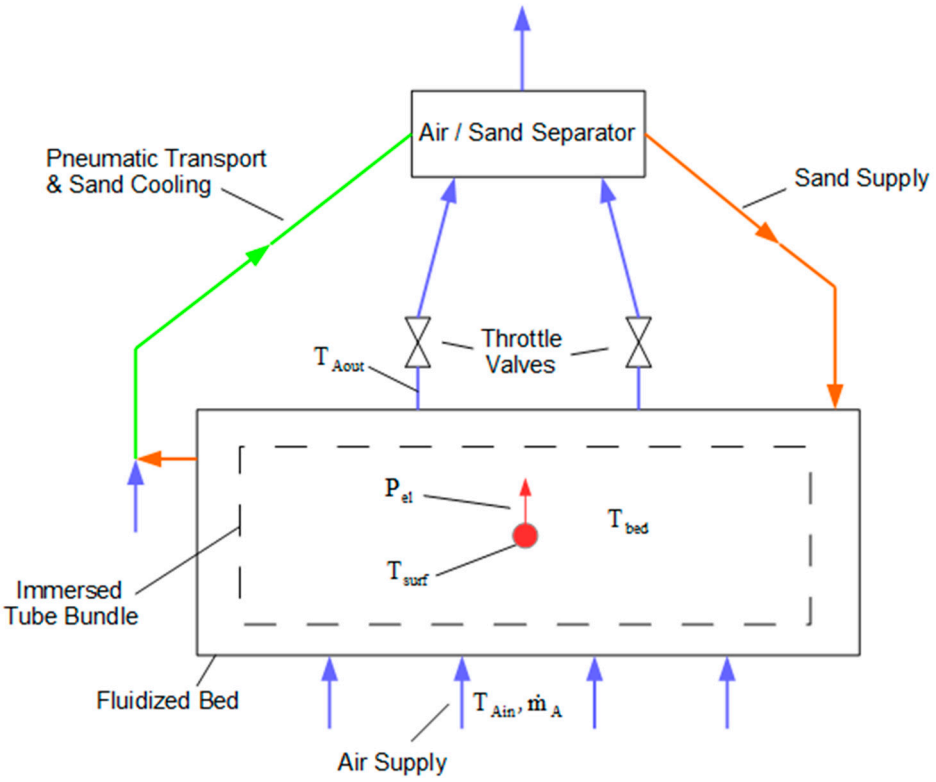

Figure 3. Generalized scheme of the test rig configuration.

Throttle valves controlled the air pressure above the fluidized bed to manage the sand level. This is the so-called air cushion technology utilized in the sandTES pilot plant [12] (pp. 89–91). Only LINI and TRINI use these valves since MICRO's cross section is too small for them to have any marked effect.

Three different sand particle sizes were investigated, with a mean particle diameter of 87 µm, 146 µm and 210 µm, respectively, and over 90% of particles within a mesh size above and below the mean particle diameter. Detailed specifications of the different particle distributions used can be found in the appendices of the respective methodology reports in the data repository.

The immersed tube bundle has a different configuration in each of the three test rigs. Although the axis of the heated tube is pictured to be perpendicular to the sand flow (TRINI), configurations with parallel tube axes were also investigated (LINI). Figure 4 shows a sketch of the heated tube in the MICRO test facility.

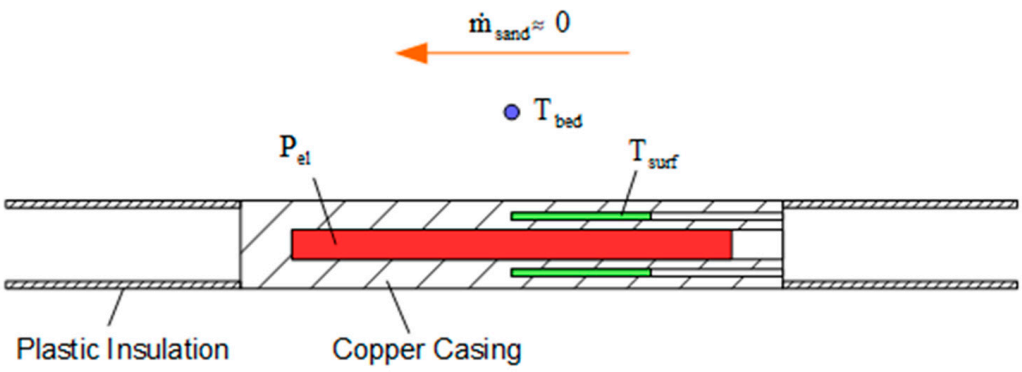

Figure 4. MICRO test tube configuration.

The electric heating cartridge (red) was placed inside a copper shell for optimized heat conduction to the surface. The copper shell was inserted between plastic tubes that

functioned as insulators to avoid any heat transfer to the walls of the fluidized bed, where the tube was mounted. Temperature sensors inside the copper shell close to the surface were used for the measurement of the surface temperature of the tube. Temperature losses due to heat conduction were ignored. MICRO is a single-cell model and the sand mass flow is very small, which is why it was used for stirred tank experiments.

The LINI test rig has a similar configuration, but with significant longitudinal sand mass flow. Additionally, longitudinal fins were investigated. A sketch of the setups is shown in Figure 5.

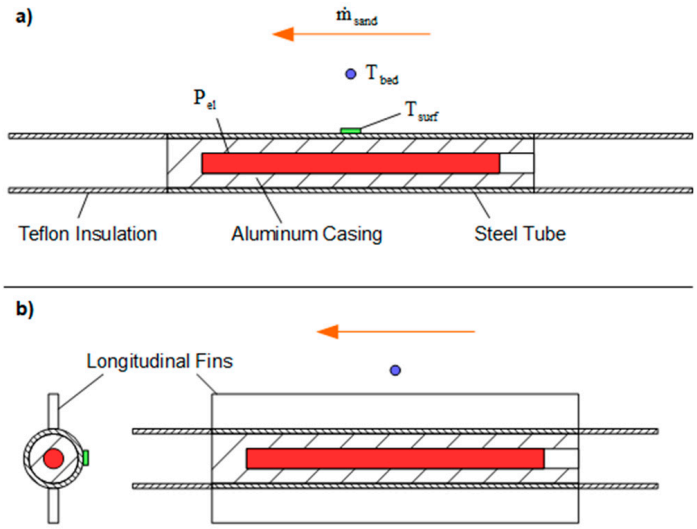

Figure 5. LINI test tube configuration: (**a**) Plain tube; (**b**) Longitudinally finned tube.

In LINI, the electric heating cartridge was placed inside an aluminum shell inside a steel tube. Using a carbon steel tube allowed the welding of the longitudinal fins (also carbon steel). The surface temperature was measured directly at the plain surface of the tube for both tube types.

The main characteristic of the TRINI test rig was its transversal sand flow, shown in Figure 6.

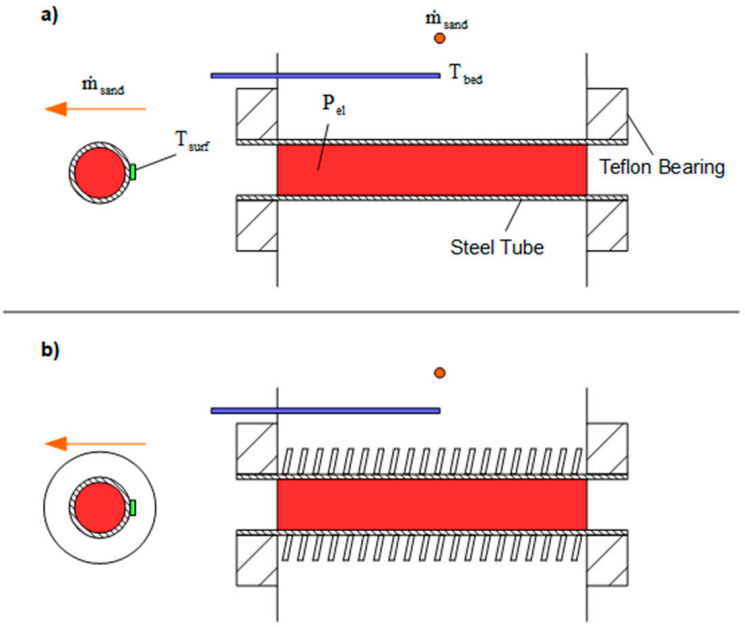

Figure 6. TRINI test tube configuration: (**a**) Plain tube; (**b**) Helically finned tube.

In the TRINI test rig, the heating cartridge was placed directly inside the steel tube. Teflon bearings had the same insulation function as the Teflon and plastic tubes used in LINI and MICRO.

The different types of fins in the LINI and TRINI test rig were chosen based on the expected flow behavior of the sand: longitudinal fins for longitudinal sand mass flow and helical fins for transversal sand mass flow. They took up the least amount of space in the respective cross section of the sand mass flow and were therefore expected to represent the smallest obstacles to it. In addition, the mainly parallel flow of particles along the fins was expected to be insensitive to erosion. The longitudinal fins of the LINI configuration only allowed for two vertical fins directly above and below the tube axis since any other number of fins or fins at a different angle would have impeded fluidization. The resulting low area multiplier was a major disadvantage of the LINI configuration compared to TRINI, see Table 1 in Section 2.2. To counteract the low area multiplier, a fin thickness of 4 mm was chosen for LINI to achieve a greater fin efficiency.

Table 1. Comparison of investigated tubes.

Test Rig	Tube Designation	Fin Configuration	Plain Area=A_{tube} (mm^2)	Fin Area (mm^2)	Area Multiplier (-)
MICRO	Plain	None	7854	0	1
LINI	Plain	None	19,635	0	1
LINI	Finned	Longitudinal, Height 18 mm, Length 250 mm, Thickness 4 mm	19,635	18,000	1.92
TRINI	Plain	None	16,965	0	1
TRINI	Finned 9/2	Helical, Pitch 9 mm, Thickness 2 mm	16,965	56,160	4.31
TRINI	Finned 9/1	Helical, Pitch 9 mm, Thickness 1 mm	16,965	54,642	4.22
TRINI	Finned 6/1	Helical, Pitch 6 mm, Thickness 1 mm	16,965	81,667	5.81

All heated tubes were placed between unheated tubes (dummies) to create a tube bundle with similar flow conditions as in an actual fluidized bed heat exchanger. Two different tube spacings were used (see Figure 7).

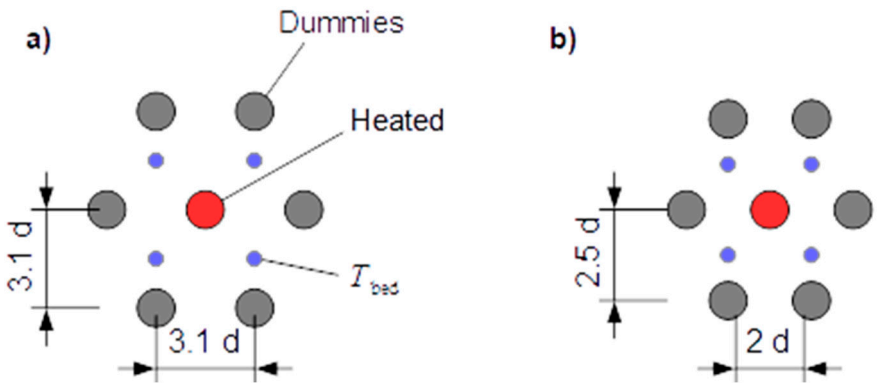

Figure 7. Investigated tube spacings: (**a**) Wide and Regular; (**b**) Narrower horizontal spacing, called sandTES tube spacing. Local bed temperature measurements were made at T_{bed}.

The given dimensions refer to a multiple of the outer tube diameter. The difference in performance between the two configurations was investigated in the MICRO test rig. All other test rigs used the sandTES tube spacing (b in Figure 7).

The TRINI test rig was also used to investigate the influence of baffles between the tubes, directing the sand in a zig-zag fashion across the tubes, as pictured in Figure 8. The use of baffles is very common in shell-and-tube heat exchangers and was previously investigated by, for example, Kong [15] and Pecora [16], with different outcomes.

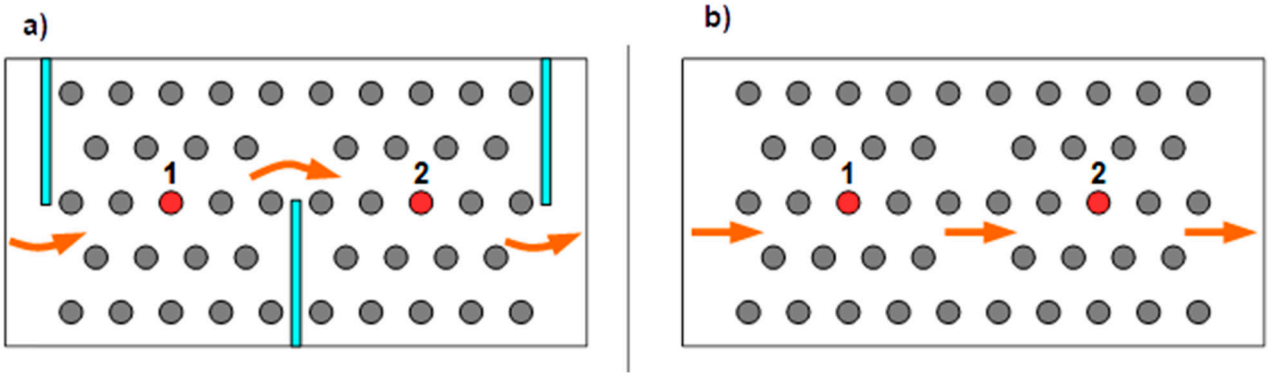

Figure 8. TRINI flow configurations: (**a**) With and (**b**) Without baffles. Both heating tubes (red, numbered 1 and 2) are active at the same time.

For this purpose, TRINI was also the only test rig employing two heated tubes, with one on each side of the baffle in the center.

2.2. Measurement and Evaluation

Two types of HTCs were measured, which are called *gross* and *net HTC*. The gross HTC is directly derived from the definition of the HTC to the surrounding fluidized bed:

$$\alpha_{gross} = \frac{P_{el}}{A_{tube}\left(T_{surf} - T_{bed}\right)} \tag{1}$$

where P_{el} is the electric power of the heating cartridge inside one of the heat exchanger tubes that heats the sand; A_{tube} is the outside surface of the heated tube; and $\left(T_{surf} - T_{bed}\right)$ is the temperature difference between the outer tube surface and the surrounding fluidized bed.

The net HTC takes the heat losses caused by the fluidization gas into account:

$$\alpha_{net} = \frac{P_{el} - \dot{m}_A \left(h_A(T_{Aout}) - h_A(T_{Ain})\right)}{A_{tube}\left(T_{surf} - T_{bed}\right)} \tag{2}$$

where $\dot{m}_A$ is the fluidization air mass flow and $(h_A(T_{Aout}) - h_A(T_{Ain}))$ is the difference in specific enthalpy of air between the outlet and inlet temperatures. Heat losses caused by the sand mass flow were ignored since the heat capacity flow of the sand far exceeded the electrical heating power, making the temperature differences of the sand across the control volume boundaries too small to measure.

Both gross and net HTC have their uses and different justifications. While the gross HTC is better suited to describe the cooling of the heated tube, the net HTC can be used to quantify the amount of heat transferred to the sand alone, which is crucial for energy storage applications. If the exhaust air is recuperated with the supplied air, as would be the case in an energy storage application, the heat losses are largely eliminated, and the net HTC is expected to be closer to the gross HTC.

The entire electric power (heat) was assumed to be transferred into the fluidized bed (sand and fluidization air), so all heat losses were ignored. This is justified by thermal

insulation of the heated pipes, as described in Section 2.1, and additional thermal insulation of the fluidized bed casing.

The thermal insulation of the heated tubes also ensured that the entire heat transfer was distributed evenly across the specified tube surface and no heat seeps into unheated parts of the heat exchanger. Otherwise, the relevant heat exchanger surface A_{tube} would be unknown.

For a better comparison of the results between plain and finned tubes, the heat exchanger surface A_{tube} is always defined as the surface of the *plain* tube, regardless of the presence of fins. The resulting HTC is thereby referred to as the *virtual* HTC. This virtual (gross or net) HTC allows direct comparison of the total length of heat exchanger tubes required for a given duty when neglecting heat conduction through the tube wall and inner HTC between tube wall and heat transfer fluid. Table 1 provides an overview of the investigated tubes.

The area multiplier is defined as the sum of plain and finned tube surface divided by the plain tube surface. The contribution of the top surface of helical fins (parallel to the tube axis) as well as the loss of heated surface at the weld seams of the fins was included in the helical fin surface.

The independent variable for the following graphs, showing the HTC-measurement results of all experiments, was the degree of fluidization, which is defined as the superficial fluidization gas velocity divided by the minimum fluidization velocity (w/w_{mf}). Using the fluidization degree FD rather than the actual superficial velocity w allowed a better characterization and comparison of the fluidization mode. Superficial velocities can always be obtained by simple multiplication of w_{mf} with FD.

Many different correlations for predicting the minimum fluidization velocity exist, such as in Richardson (1971) [17] (p. 70), but experimental examination is usually considered to be more accurate. However, to ensure better comparability between the results in the different test rigs, the minimum fluidization velocity was calculated the same way for all test rigs, using Richardson's correlation:

$$w_{mf} = \mathrm{Re}\,\frac{\eta_g}{d_p\,\rho_g}$$
$$\mathrm{Re} = \sqrt{C_1{}^2 + C_2\,\mathrm{Ar}} - C_1$$
$$\mathrm{Ar} = \frac{\rho_g\,{d_p}^3\,(\rho_p - \rho_g)g}{{\eta_g}^2}$$

where w_{mf} is the minimum fluidization velocity; Re is the Reynolds number; η_g is the dynamic viscosity of the fluidization gas; ρ_g is the fluidization gas density; d_p is the mean particle diameter; Ar is the Archimedes number; and g is the gravitational acceleration. The constants $C_1 = 25.7$ and $C_2 = 0.0365$ were set according to Richardson.

This correlation was chosen over others because it proved to be in fairly good agreement with the actual minimum fluidization velocity in other test rigs in previous experiments. By using the same correlation for all test rigs, the net HTCs were calculated with about the same mass flow for all since fluidization air temperature was also roughly the same for all (slightly above ambient temperature). This made net HTCs for identical particle diameters directly comparable.

3. Results

3.1. General

The results of the experiments presented in this paper are the findings of a largely phenomenological investigation. The main goal was to identify quantitative differences in the heat transfer characteristics in fluidized beds between different types of tube bundle configurations and different particle sizes. Developing new correlations for the heat transfer coefficient between a tube's outer surface and the surrounding fluidized bed (e.g., for finned tubes) is outside the scope of this investigation.

However, to help the reader to interpret the results, regression curves are introduced in all graphs. The underlying hypothesis of all experiments is that the heat transfer coefficient

would at first increase with the degree of fluidization, experience a maximum value, and then decrease again. For this reason, a second order polynomial was fitted to all results using the method of least squares. The values of R^2 (the coefficient of determination) given in the figure legends then indicate how well the respective data fits the hypothesis.

The error bars in the following figures refer to the scatter of the measurements taken at varying degrees of fluidization. For the measurement uncertainties, see Appendix A.

3.2. MICRO Test Rig

First, the performance of the different tube spacings was investigated in the MICRO test rig. The results for the regular tube spacing are shown in Figure 9.

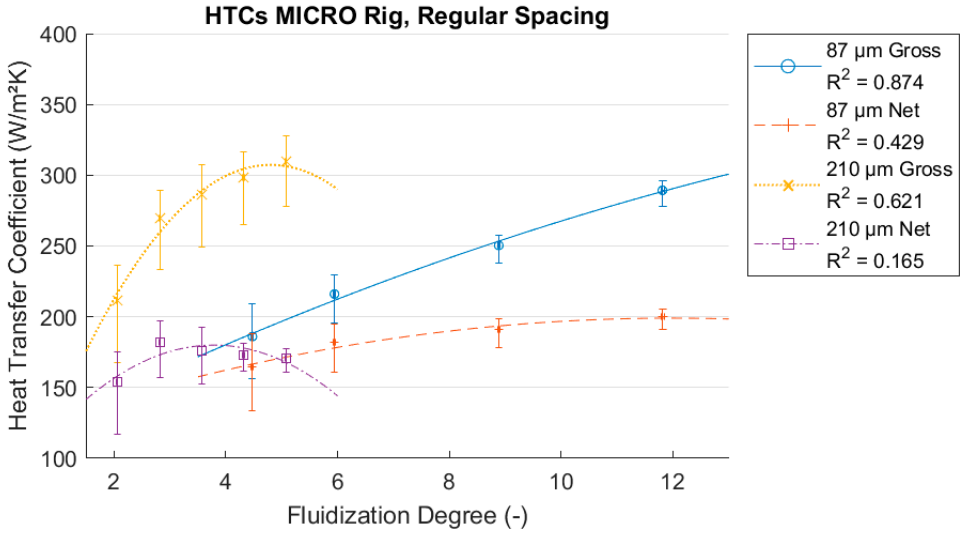

Figure 9. HTCs MICRO rig, Regular Spacing, $w_{mf}(87\ \mu m) = 7.6\frac{mm}{s}$, $w_{mf}(210\ \mu m) = 43.7\frac{mm}{s}$.

One can see that the gross HTCs of the 87 µm sand increase almost indefinitely with rising degrees of fluidization. This shows that the tube is cooled better with increasing air mass flow, as was to be expected. In comparison, the net HTC decreases quicker, although its maximum value is probably outside the boundaries of the graph. The gross HTC of the 210 µm sand shows a much steeper inclination and likely has a peak value at a degree of fluidization between 5 and 6. Its net HTC shows a maximum within the measured range at a degree of fluidization of around 4. The differences between the gross and net HTC are much greater in the case of the 210 µm sand than with the 87 µm sand, indicating greater heat losses when using coarser particles. Due to the very low minimum fluidization velocity of the 87 µm sand, it was not possible to observe lower degrees of fluidization.

The results of the same experiments with the sandTES tube spacing are shown in Figure 10.

The heat losses appear to be greater than with the regular tube spacing, in particular when using 210 µm sand, where the heat losses are disproportionate and the net HTC decreases steadily. The net HTC of the 87 µm sand seems to decrease faster than with the regular tube spacing shown in Figure 9 and has a maximum value at a lower degree of fluidization.

In comparison, the sandTES tube spacing performs consistently better than the regular tube spacing within the limits of the measured degrees of fluidization. Therefore, the better performance of the sandTES tube spacing seems to be confirmed by the results of these experiments. This is why it was decided to conduct experiments with the sandTES tube spacing only from this point on.

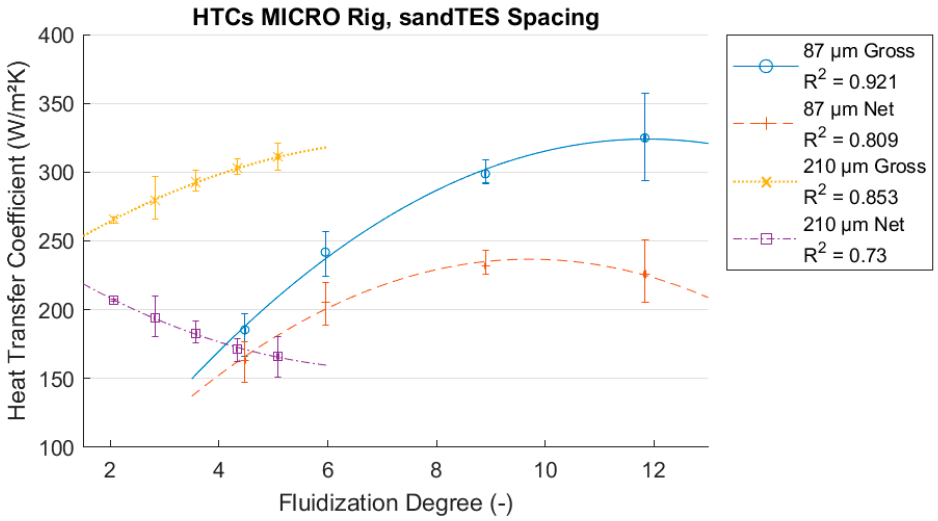

Figure 10. HTCs MICRO rig, sandTES Spacing, $w_{mf}(87\ \mu m) = 7.6\frac{mm}{s}$, $w_{mf}(210\ \mu m) = 43.7\frac{mm}{s}$.

Both figures show that at lower degrees of fluidization, where a fluidized bed would usually be operated, the coarser sand seems to perform better than the finer sand in terms of achievable HTC. As mentioned in Section 2.2, in an energy storage application with recuperated (hot) fluidization gas, the net HTC is expected to be closer to the gross HTC. However, larger particle diameters greatly increase the power required for fluidization, lowering the efficiency of an energy storage system. This auxiliary power is proportional to the minimum fluidization velocity (which is proportional to the particle diameter) and the degree of fluidization. The greater required air mass flow for fluidization is also represented by the greater difference between gross and net HTC of the 210 µm sand compared to the 87 µm sand, which results from greater heat losses. Therefore, a compromise was made and sand with a mean particle diameter of 146 µm was used in all experiments from this point on.

3.3. LINI Test Rig

The results of the LINI test rig (sandTES spacing, 146 µm particle diameter) are shown in Figure 11.

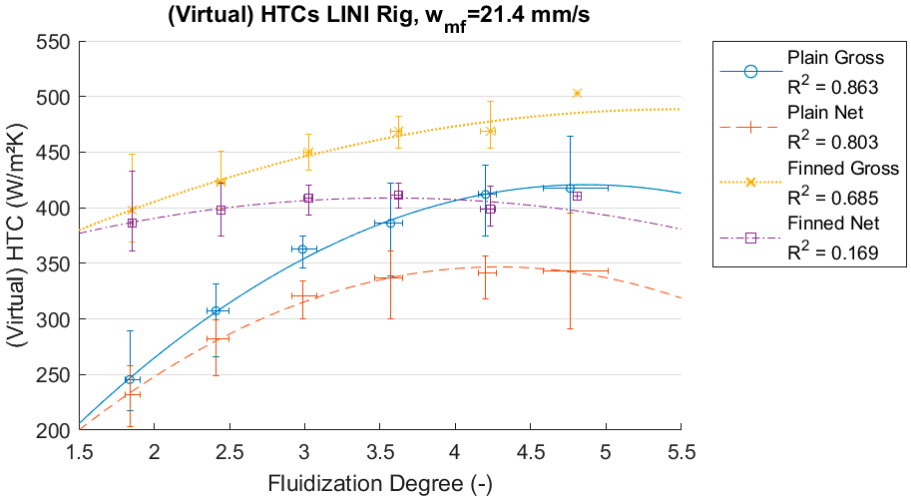

Figure 11. Results of the LINI test rig, plain and finned tubes, 146 µm particles.

The net HTC seems to decrease beyond a degree of fluidization of around 4 to 5, which is a good operational value, although measurements at higher degrees of fluidization are

missing for a definitive conclusion. Compared to the MICRO experiments with 210 µm sand, the HTCs are slightly better, in particular the net HTC, which is not very surprising given the lower air mass flow required for the same degree of fluidization.

One can see that the finned tubes perform better than the plain tubes, especially at lower degrees of fluidization. The difference between gross and net HTCs is slightly increased in the case of the finned tubes compared to plain tubes, which is likely due to the larger total heat transfer area. However, the finned tubes were unable to increase maximum performance significantly.

3.4. TRINI Test Rig

First, plain tubes were investigated to compare with the results from the MICRO and LINI test rigs. As described in Section 2.1, Figure 8, two heat exchanger configurations were investigated to determine the difference in performance when putting vertical baffles between the heat exchanger tubes. The results are shown in Figures 12 and 13.

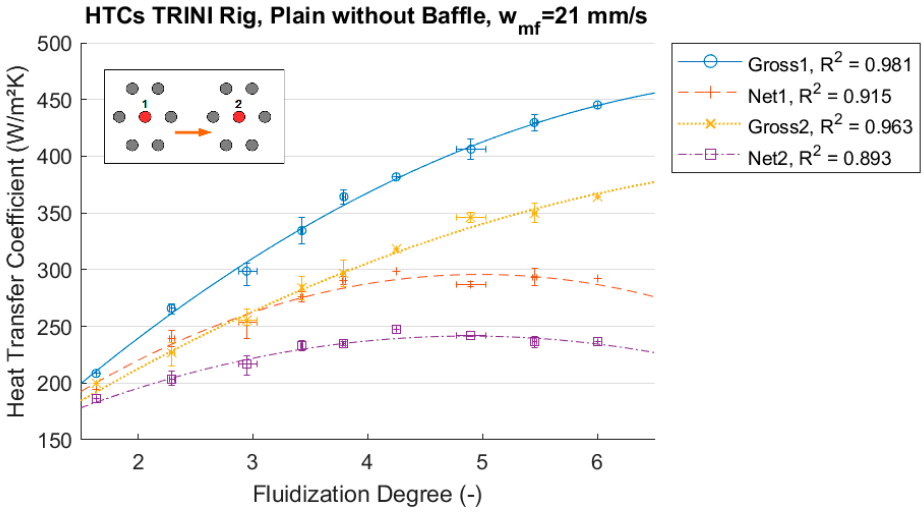

Figure 12. Plain tube results without the use of baffles, TRINI test rig, 146 µm particles. Indices 1 and 2 refer to the different heated tubes.

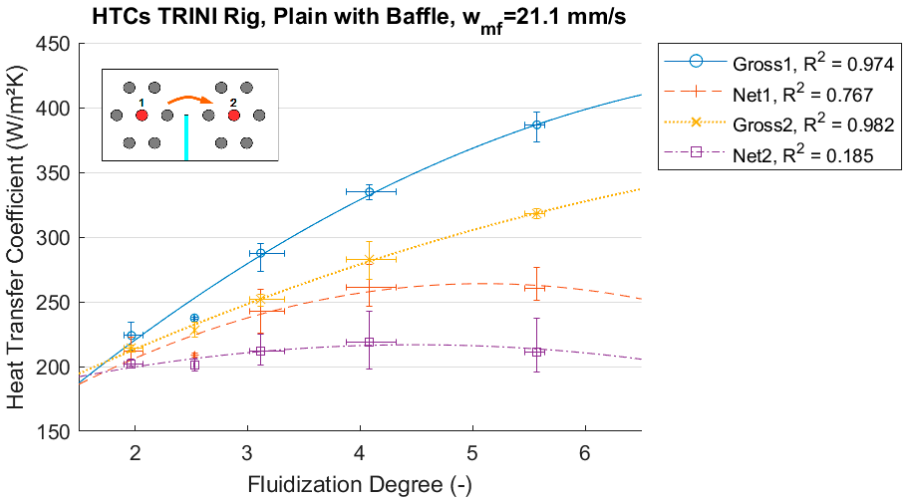

Figure 13. Plain tube results when using baffles, TRINI test rig, 146 µm particles. Indices 1 and 2 refer to the different heated tubes.

The numbers in the legends of the two graphs refer to the respective heat exchanger tube: 1 for the tube upstream of the center baffle, and 2 for the one downstream (Figure 8).

It is not entirely clear why the two tubes show significantly different values, while both their heat transfer behaviors seem qualitatively similar and consistent within themselves. The influence of the baffle could be an explanation in the case of those experiments that included it, but not for the ones that did not. It is possible that the local fluidization around the respective sensors was different or that the produced heat from the heating cartridge was distributed unevenly and dissimilar in both tubes. Localized sand flows might have also played a role.

In general, longitudinal flow conditions (LINI) seem to yield slightly better results when using plain tubes at comparable degrees of fluidization and the same particle size compared to the transversal flow conditions shown here.

A comparison of the two configurations is shown in Figure 14, where the mean of the respective gross and net HTCs were taken to provide a better overview.

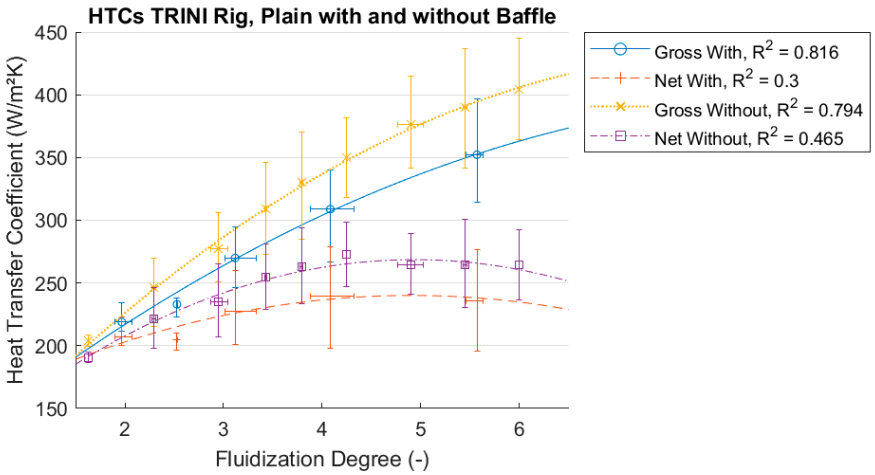

Figure 14. Comparison of the results with and without the use of a baffle, TRINI test rig, 146 µm particles.

One can see that the average heat transfer coefficients are higher when no baffle is used. This confirms the original hypothesis that baffles hinder the performance of the heat exchanger, likely by creating a series of stirred tanks. Therefore, all other experiments from this point on were conducted without the use of baffles.

The results of the two fin configurations with a fin spacing of 9 mm and fin thickness of 2 mm and 1 mm (9/2 and 9/1) are shown in Figures 15 and 16.

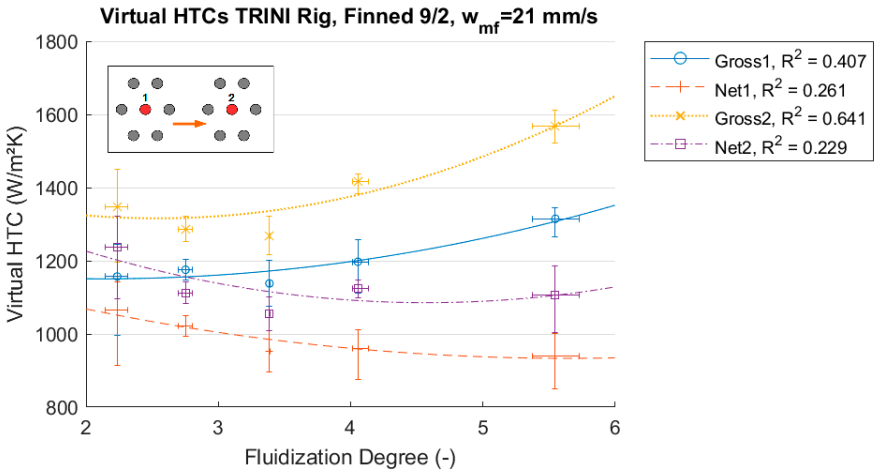

Figure 15. Results of helically finned tubes, pitch 9 mm, fin thickness 2 mm, TRINI test rig, 146 µm particles. Indices 1 and 2 refer to the different heated tubes.

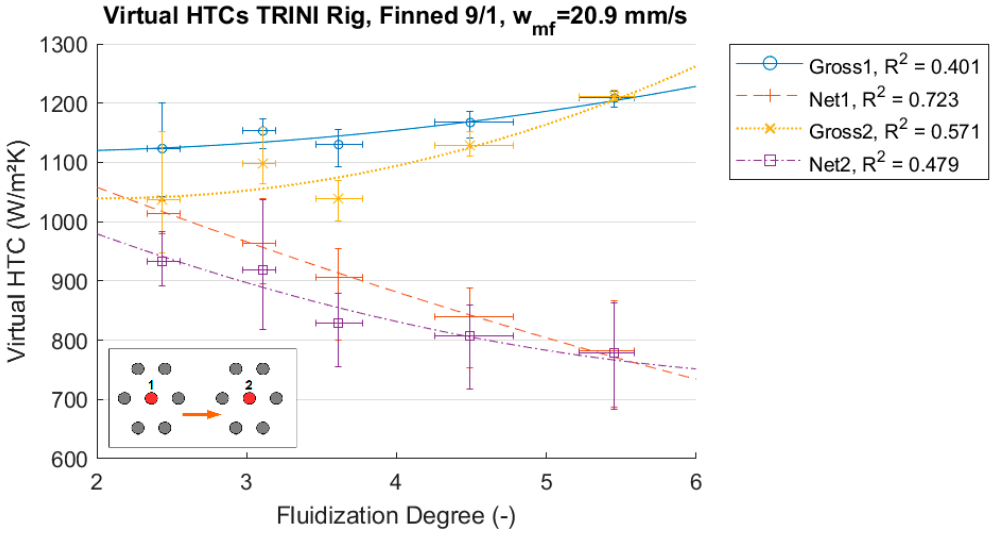

Figure 16. Results of helically finned tubes, pitch 9 mm, fin thickness 1 mm, TRINI test rig, 146 µm particles. Indices 1 and 2 refer to the different heated tubes.

A similar discrepancy between the results of the two heated tubes can be observed as with the plain tubes, though the first tube shows better results than the second tube in the case of the 1 mm thick fins. A direct comparison between the two fin configurations is shown in Figure 17.

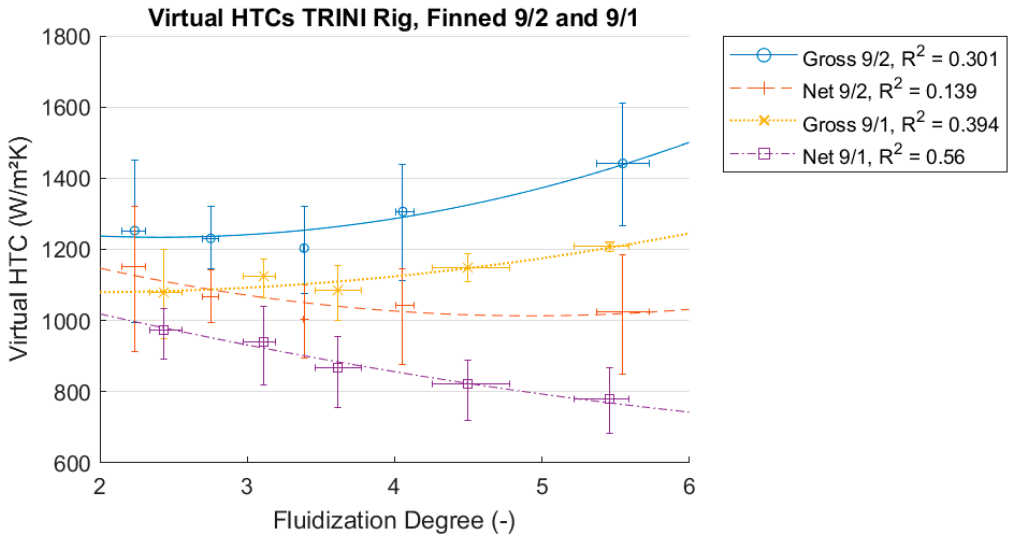

Figure 17. Comparison between 1 mm and 2 mm thick helical fins, TRINI test rig, 146 µm particles.

The results represent the mean values between the two tubes in the respective configuration. Clearly, the 2 mm thick fins show higher HTCs in general and a more stable net HTC than the 1 mm thick fins, which is not surprising given the lower fin efficiency of thinner fins [18] (pp. 1273–1274).

The results of the last fin configuration with a fin spacing of 6 mm and a fin thickness of 1 mm are shown in Figure 18.

This is the only graph where a first order polynomial was used for the regression analysis. The results of this experiment are inconsistent with the previous results (the gross heat transfer coefficient decreases with increasing degree of fluidization) and show a much greater variability. It is believed that the small distance between the fins caused local disturbances in the sand flow, leading to bad results. The results of this experiment are therefore not taken into account.

Finally, Figure 19 shows the comparison between the best performing finned tubes (9/2) and plain tubes.

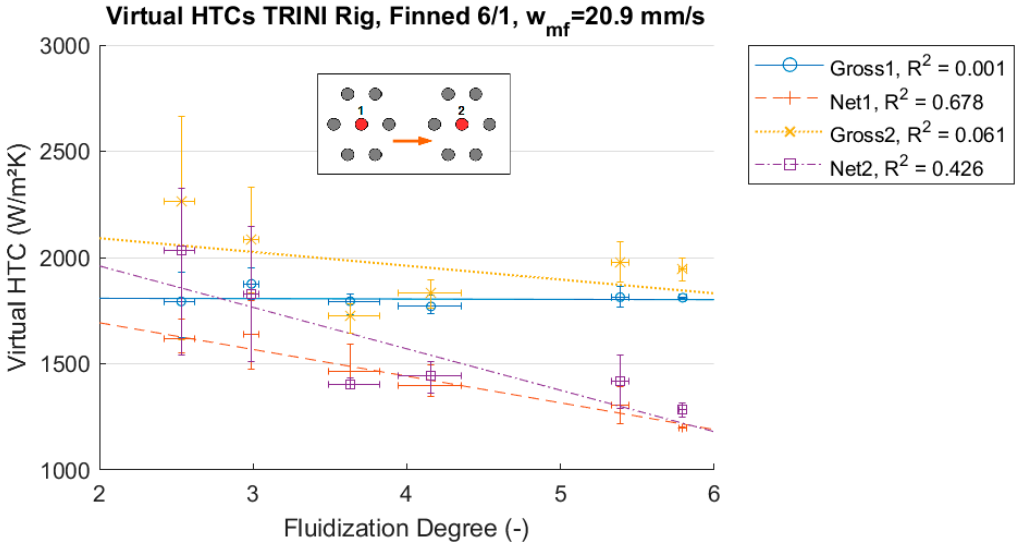

Figure 18. Results of helically finned tubes, pitch 6 mm, fin thickness 1 mm, TRINI test rig, 146 µm particles. Indices 1 and 2 refer to the different heated tubes.

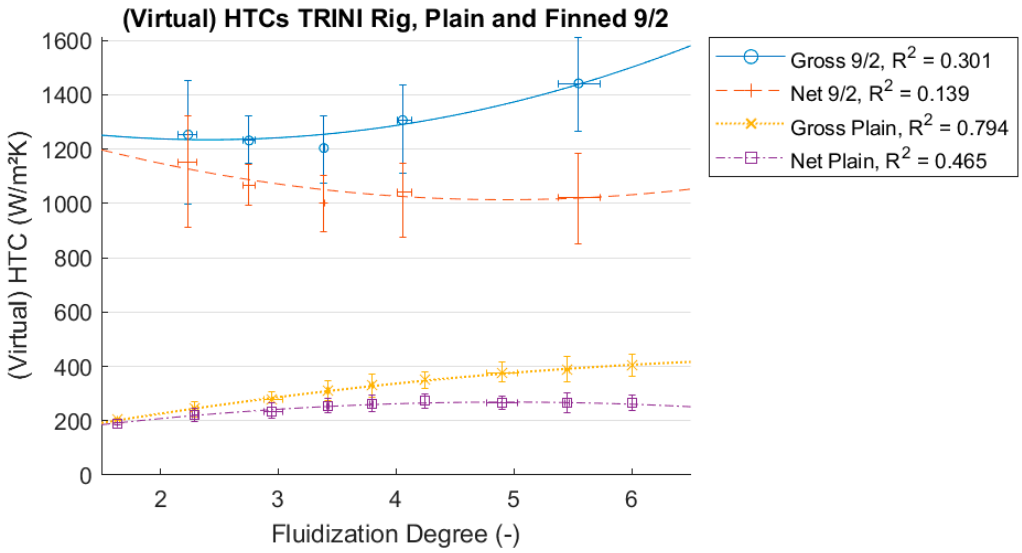

Figure 19. Comparison between plain and helically finned tubes, pitch 9 mm, thickness 2 mm, TRINI test rig, 146 µm particles.

At the most promising degree of fluidization of 4, the finned tubes show a (virtual) HTC about 3.5 times greater than that of the plain tubes. Given that the area multiplier of the 9/2 fin configuration is 4.31 (see Table 1), the effective fin efficiency is about 81%.

4. Discussion

As mentioned in the Introduction, several correlations for predicting the heat transfer between an immersed surface and the surrounding fluidized bed exist, but none of them consider finned tubes or an imposed horizontal mass flow. Therefore, only the plain tube results of the individual test rigs may be compared to these correlations, for which three were chosen:

- Grewal [4], which is based on the correlations by Andeen and Glicksman [2] and Bansal [3], utilizes the boundary layer approach. It considers horizontal tube banks and takes the pitch between the tubes into account:

$$\mathrm{Nu} = 47(1-\varepsilon)\left(\frac{w\ d_T\ \rho_p}{\mu_g}\ \frac{{\mu_g}^2}{{d_p}^3{\rho_p}^2 g}\right)^{0.325}\left(\frac{\rho_p c_p {d_T}^{\frac{3}{2}} g^{\frac{1}{2}}}{\lambda_g}\right)^{0.23}\left(\frac{\mu_g c_g}{\lambda_g}\right)^{0.3}\left(1-0.21\left(\frac{P}{d_T}\right)^{-1.75}\right)$$

where $\mathrm{Nu} = \alpha d_T/\lambda_g$ is the Nusselt number; α is the HTC; d_T is the tube diameter; λ is thermal conductivity; ε is the mean bed porosity; w is the superficial fluidization velocity; ρ is density; μ is dynamic viscosity; d_p is the mean particle diameter; g is gravitational acceleration; c is specific heat capacity; and P is the tube pitch (distance between tubes in a bundle). The subindex p stands for particle properties, while the subindex g denotes fluidization gas properties.

Since Grewal's correlation only considers uniform tube spacing (only a single value P is used for the tube pitch, so no difference between the horizontal and vertical pitch is considered), the mean pitch is taken when applying this formula to the sandTES pitch.

It is important to mention that the heat transfer coefficient decreases with the smaller pitch according to this correlation.

- Martin [7] uses a kinetic model. The numerous formulas required are given in the methodology report in the repository. Its main parameters are particle size, density, thermal conductivity, heat capacity and fluidization gas pressure as well as bed porosity and temperature.
- Molerus [5] combines both particle and gas heat transfer based on a characteristic length l:

$$l = \left(\frac{\mu_g}{\sqrt{g}\left(\rho_p - \rho_g\right)}\right)^{\frac{2}{3}}$$
$$\frac{1}{\alpha} = \frac{l}{0.09\lambda_g} + \frac{l}{0.09 c_p \mu_g}$$

The definition of the symbols is the same as for Grewal above.

All the correlations above depend on the mean bed porosity, which was estimated based on the fluidization velocity:

$$\mathrm{Ar} = \frac{\rho_g {d_p}^3\left(\rho_p - \rho_g\right) g}{{\mu_g}^2}$$
$$\mathrm{Re}_p = \frac{w\ d_p\ \rho_g}{\mu_g}$$
$$\varepsilon = \left(\frac{0.36\ {\mathrm{Re}_p}^2 + 18\ \mathrm{Re}_p}{\mathrm{Ar}}\right)^{0.21}$$

where Ar is the Archimedes number and Re_p is the particle Reynolds number.

The comparison for the MICRO tests can be seen in Figures 20 and 21.

One can see that all correlations severely overestimate the achievable heat transfer coefficient in the case of the 87 µm particles by a factor of about 2–3. This may have been caused by the use of very small particles that are at the border of Geldart region [19] A. In the case of the 210 µm particles, only Grewal's correlation shows a fairly good agreement with the results. However, Grewal predicts almost identical heat transfer when using either the regular tube spacing or the sandTES tube spacing (regular is always slightly greater), while the experiments showed better results when using the sandTES tube spacing over a wide range of fluidization degrees. This may be the result of the lower tubes in the bundle redirecting the bed bubbles toward the heated tube, thereby increasing the bubble frequency and particle renewal rate there.

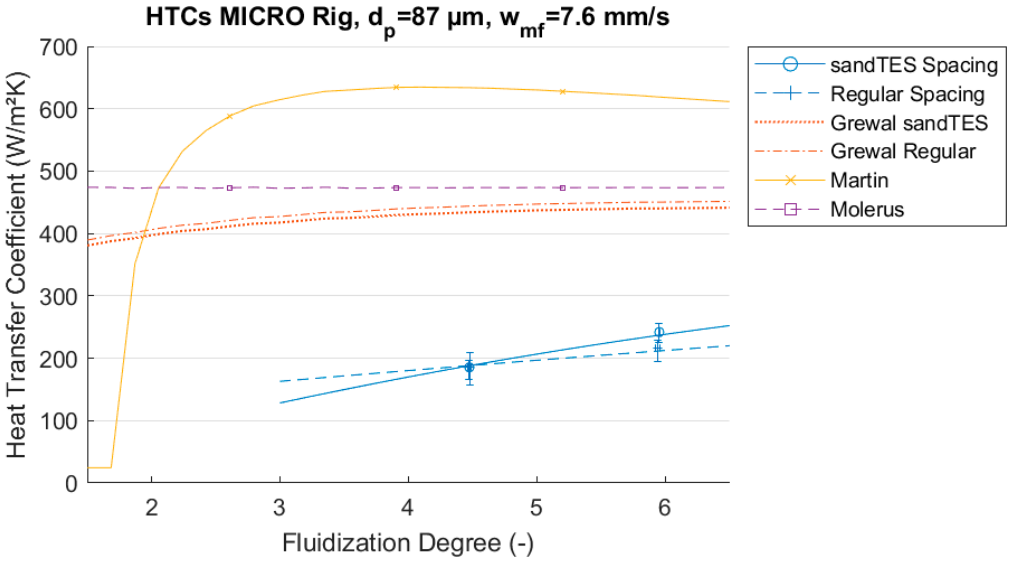

Figure 20. Comparison of MICRO results with 87 µm particles.

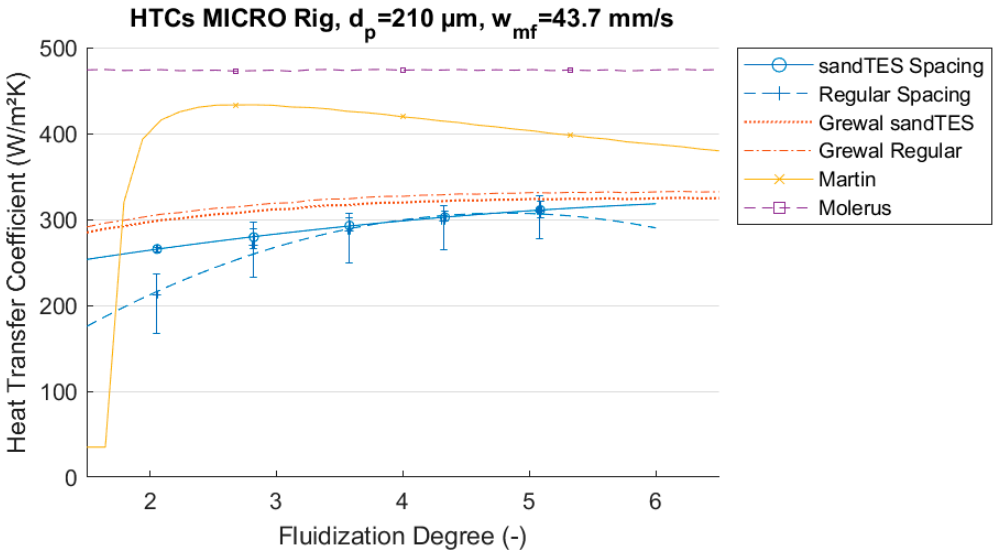

Figure 21. Comparison of MICRO results with 210 µm particles.

Martin overestimates the minimum fluidization velocity in the case of the 210 µm particles, resulting in a sharp increase in predicted heat transfer coefficients only at a degree of fluidization of about 1.5. This is caused by the correlation for the estimation of the bed porosity that predicts porosities lower than the (measured) 45% at very low fluidization. To ensure a consistent use of the porosity correlation across all HTC correlations, bed porosity in Martin's correlation was kept at a minimum of 45% to overcome numerical issues. See the methodology report in the repository for details.

While Molerus is close to Grewals's predictions in the case of the 87 µm particles, it is very far away in the case of 210 µm particles. This demonstrates the great discrepancies between correlations often encountered when trying to predict heat transfer in a fluidized bed.

Figures 22 and 23 show the comparisons of the LINI and TRINI results to the different correlations:

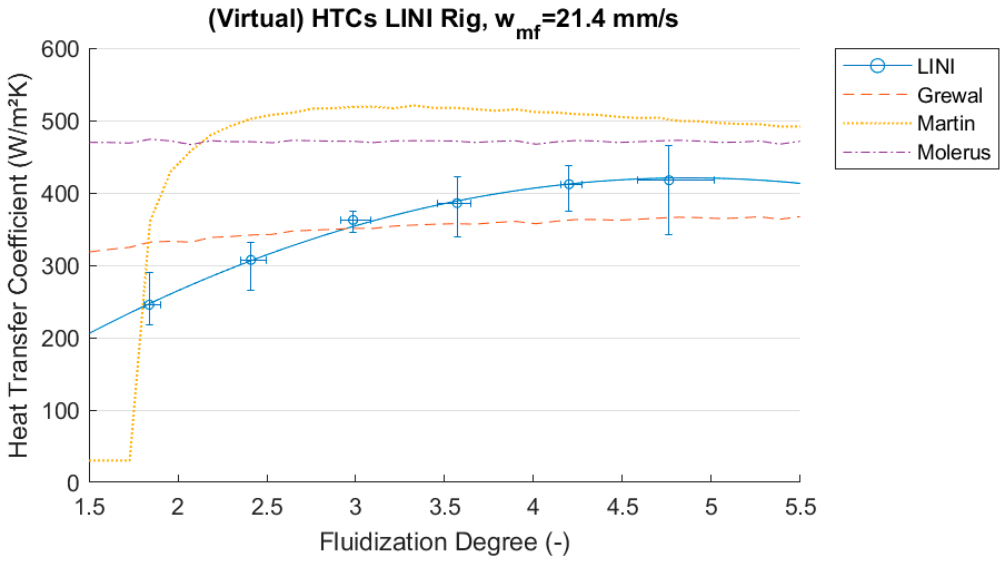

Figure 22. Comparison of LINI results, 146 µm particles.

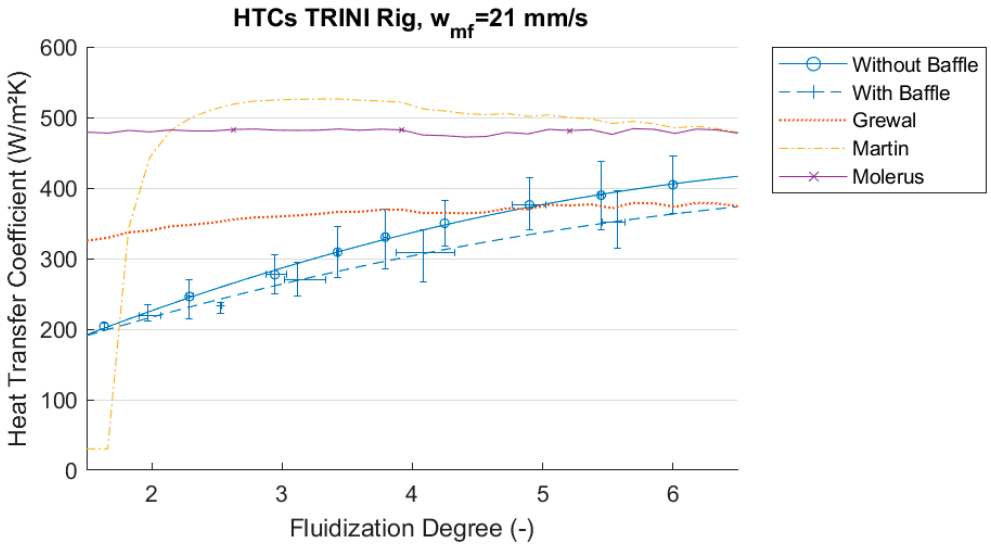

Figure 23. Comparison of LINI results, 146 µm particle.

Although the correlations seem closer to the measurements for higher degrees of fluidization, they all overestimate the heat transfer at lower degrees of fluidization. The range between predicted values is still very larger for reliable design considerations.

The main findings of the experiments are:

- The narrower tube spacing, referred to as the sandTES tube spacing with a relative horizontal pitch of 2.0 and a relative vertical pitch of 2.5, has a slightly better performance than the regular tube spacing with a relative pitch of 3.1 in both the horizontal and vertical direction. This confirms the conclusion drawn from the CPFD simulations by Schwaiger [12] (p. 170). This may be explained by tubes in the bundle increasing the local bubble frequencies at tubes above them by redirecting the bubbles towards them. An increased bubble frequency is related to higher HTCs in the correlation by Mickley and Fairbanks, and a narrower tube spacing has a better chance of individual tubes influencing the local bubble frequency at other tubes than a wider spacing.
- Finned tubes with a fin pitch of 9 mm and fin thickness of 2 mm in a transversal arrangement in respect to the sand mass flow show a 3–6 times greater (virtual) HTC

than plain tubes in the same arrangement. At a degree of fluidization of about 4, the factor is about 3.5 at 1250 W/m^2K (gross) in respect to the plain tube surface.

- The use of baffles in between tubes in a transversal arrangement seems to decrease the achievable HTC.

In the intended thermal energy storage application, the fluidized bed would be operated at significantly higher temperatures (compared to the experiments that were conducted at about 40 °C) and the thermal energy of the exhausted fluidization air would be recuperated with the supply air. The net HTC, which only accounts for the heat directly transferred into the storage material (sand), is then expected to increase and be closer to the gross HTC. The reason for this is that heat losses through fluidization depend on the mass flow of the fluidization gas while the degree of fluidization depends on fluidization gas velocity. Since gas density decreases with rising temperatures, a lower mass flow is required to achieve the same degree of fluidization:

$$\frac{\dot{m}_A(T)}{\dot{m}_A(T_0)} = \frac{w_{mf}(T)\,\rho(T)}{w_{mf}(T_0)\,\rho(T_0)}$$

where w_{mf} is the minimum fluidization velocity gathered from Richardson's correlation. For dry air at ambient pressure as fluidization gas and T_0 = 40 °C, the relation is shown in Figure 24.

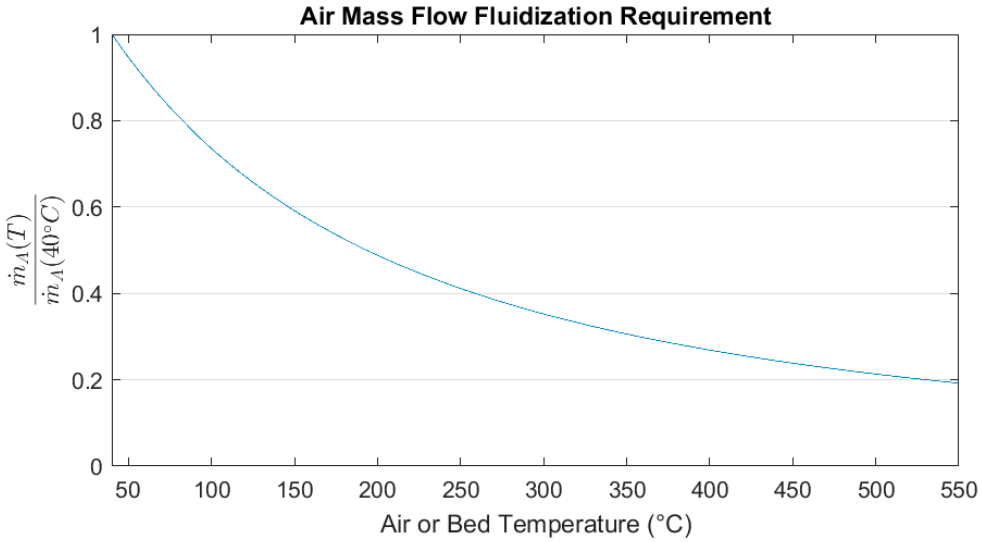

Figure 24. Required fluidization air mass flow depending on temperature relative to 40 °C.

It is clear that the required mass flow decreases very quickly with the rising temperature. At 400 °C, only about 27% of the original air mass flow at 40 °C is required to achieve the same degree of fluidization. In this way, the net HTC approaches the gross HTC with increasing temperatures. When the lost thermal energy caused by the fluidization is recuperated with the supplied air, heat losses can be further decreased and the net HTC moves even closer to the gross HTC.

In the experimental work of this paper, the differences in particle convective heat transfer for different geometries and particle flow arrangements at temperatures slightly above ambient temperature (40 °C) was determined. In order to estimate the temperature dependence of the HTC, several of the aforementioned correlations were investigated in respect to their sensitivity to temperature changes, namely the ones by Andeen and Glicksman [2], Grewal [4], Molerus [5], Zabrodsky [20], Martin [7], and Gelperin and Einstein [21]. Unfortunately, there are great discrepancies between the predictions, as shown in Figure 25.

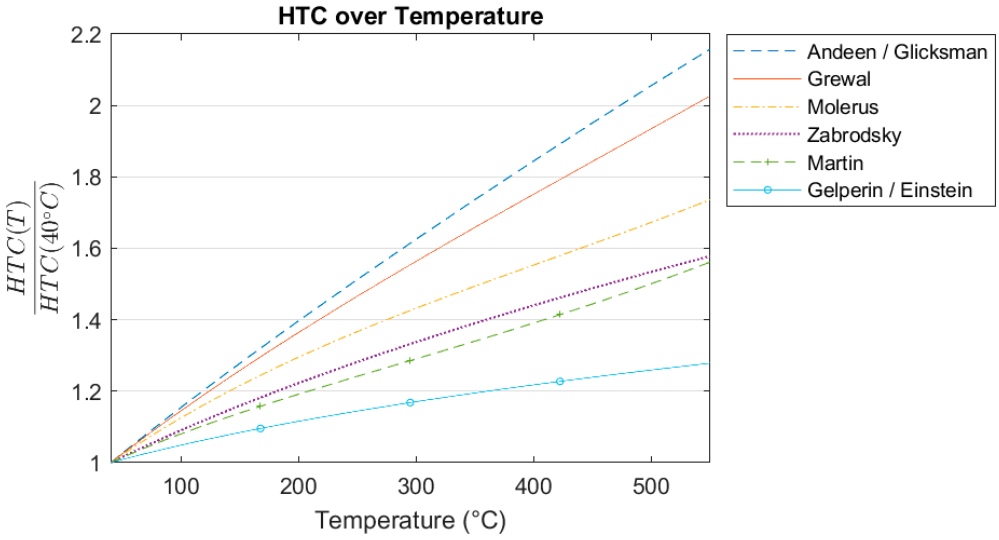

Figure 25. Comparison of HTC correlations depending on temperature, relative to 40 °C.

The "packet model" by Mickley and Fairbanks [6] and the correlation by Bansal [3] show almost identical results to the correlation by Andeen and Glicksman. Using the correlation by Zabrodsky, since it represents a good average between the different correlations, the HTC at 400 °C is expected to be 1.44 times the one at 40 °C.

This study revealed several issues for additional research:

- It is unclear whether the performance of the sandTES tube spacing was influenced by the irregular pitches in the vertical (2.5 times the tube diameter) and horizontal (2 times) directions and whether a regular but still narrower tube spacing than the one investigated (3.1 times in both directions) could improve the results.
- Vertical mixing greatly exceeds the horizontal movement of the fluidized bed [22], which is why the dependence of the HTC on the magnitude of horizontal sand mass flow is expected to be low and was largely ignored in this study. However, the flow conditions of the fluidized bed apparently cannot be ignored, as the results of the experiments with (LINI, TRINI) and without (MICRO) significant sand mass flow and the difference between the experiments with and without baffles (TRINI) show. The sand mass flow might play a role in the formation of these flow conditions and should be investigated.
- The discrepancy between the results of the different heated tubes in the TRINI test rig was also likely caused by local flow conditions or disturbances.
- The test rigs were designed in such a way that the sand mass flow could not be controlled and established itself independently. The degree of fluidization might have an impact on the apparent viscosity of the fluidized bed and thereby might have influenced the sand mass flow in the test rigs. In this case, if the sand mass flow has an influence on HTCs, the degree of fluidization could have had an impact on HTCs through the alteration of the sand mass flow. Because of this, the influence of the degree of fluidization on apparent viscosity of the fluidized bed should be investigated.
- It is expected that the horizontal sand mass flow should at least exceed the temperature dispersion in the fluidized bed in the opposite flow direction. However, the required apparent heat conduction (through sand and fluidization gas as a quasi-homogenous material) is unknown and should be investigated.
- Since the experiments were only conducted at temperatures slightly above ambient temperature, experiments at the expected operating temperatures of a thermal energy storage system should be conducted.
- Additional research is needed to find a correlation for reliable predictions of HTCs at higher temperatures to reconcile the differences shown in Figure 25.

- A generalized model for predicting flow conditions and HTCs based on an arbitrary set of boundary conditions is still needed and could not be deduced from the experiments in this study alone.

5. Conclusions

The conducted experiments showed that a transversal flow arrangement, where the horizontal flow direction of the sand is perpendicular to the tube axes, and helically finned tubes greatly increase the virtual HTC compared to other tube configurations. Narrower tube spacings seem to improve the HTC while the use of baffles deteriorates it. The achieved virtual gross HTC in the range of 1250 W/m^2K at a degree of fluidization of about 4 allows the design and construction of compact, low-cost heat exchangers and is expected to further increase with higher operating temperatures.

The analysis of the results and comparison to previously published work demonstrated that many of the currently available methods for predicting the heat transfer behavior in a fluidized bed deliver results with great variance, in particular when it comes to the dependence on operating temperature. This stresses the need for further research in the field.

6. Patents

The intellectual property of the following patents was utilized and further developed: HEAT STORE SYSTEM, WO 2012/027769 A2; GAS DISTRIBUTION DEVICE, WO 2015/172172 A4; FLUIDIZED BED REACTOR WITH HORIZONTAL DIRECTION, WO 2015/188214 Al.

Author Contributions: Conceptualization, S.T.; methodology, S.T.; software, S.T.; validation, S.T. and P.S.; formal analysis, S.T. and P.S.; investigation, S.T.; resources, M.H.; data curation, S.T. and P.S.; writing—original draft preparation, S.T.; writing—review and editing, M.H.; visualization, S.T.; supervision, M.H.; project administration, S.T. and M.H.; funding acquisition, M.H. All authors have read and agreed to the published version of the manuscript.

Funding: The information, data, or work presented in this paper was funded in part by the Advanced Research Projects Agency-Energy (ARPA-E), U.S. Department of Energy, under Award Number DE-AR0000996. The views and opinions of authors expressed herein do not necessarily state or reflect those of the United States Government or any agency thereof. The APC was funded by TU Wien Bibliothek.

Institutional Review Board Statement: Not applicable.

Informed Consent Statement: Not applicable.

Data Availability Statement: The data presented in this study are openly available in Zenodo at https://doi.org/10.5281/zenodo.5890230 (20 December 2021), Experimental Investigation of the Heat Transfer between Finned Tubes and a Bubbling Fluidized Bed with Horizontal Sand Mass Flow (data set). Software for data analysis is openly available in Zenodo at https://doi.org/10.5281/zenodo.5500329 (20 December 2021), sthanhe/HeatTransfer: Round 3 Release (V1.0.3).

Acknowledgments: Dominik Groicher and Fabian Bärnthaler collected data; Verena Sulzgruber, Lukas Pöppel and David Kerekes supported the engineering of test rigs; and Florian Heindl supported the methodology with simulations. Echogen Power Systems, the prime awardee of DE-AR0000996, supported this work with regard to project administration and funding acquisition. The authors acknowledge TU Wien Bibliothek for financial support for editing/proofreading and its Open Access Funding Programme.

Conflicts of Interest: The authors declare no conflict of interest. The funders had no role in the design of the study; in the collection, analyses, or interpretation of data; in the writing of the manuscript, or in the decision to publish the results.

Appendix A

Table A1 shows the measurement uncertainties of the different test rigs.

Table A1. Measurement uncertainties.

Rig	Set Series	FG			Alpha_Gross			Alpha_Net		
		Min	Mean	Max	Min	Mean	Max	Min	Mean	Max
MICRO	87 µm Regular	1.63	2.26	3.73	5.72	6.24	6.82	12.03	16.41	21.72
	87 µm sandTES	1.63	2.57	3.73	5.67	6.12	6.67	11.81	15.15	20.54
	210 µm Regular	1.37	1.43	1.64	5.85	6.37	6.98	22.64	35.85	50.66
	210 µm sandTES	1.37	1.43	1.64	5.84	6.38	6.94	19.60	34.90	57.27
LINI	Plain	1.13	1.24	1.61	3.24	3.79	4.78	3.84	5.33	7.95
	Finned	1.13	1.25	1.61	3.08	3.42	4.16	3.36	4.30	6.35
TRINI	Plain Without	16.15	29.97	58.21	3.22	3.70	6.25	7.36	12.19	16.98
	Plain With	16.15	30.61	58.21	3.03	3.49	6.25	5.69	11.51	17.52
	Finned 9/2	16.65	29.44	44.76	4.81	5.45	6.19	9.79	12.47	17.66
	Finned 9/1	17.54	27.56	42.37	5.19	6.09	7.46	8.58	15.54	26.08
	Finned 6/1	16.76	26.75	39.46	6.84	8.28	11.97	10.49	16.22	20.37

All values are in percent of the respective measured value. They can refer to both positive and negative deviations. All measurement uncertainties are additionally documented in the form of graphs in the data repository.

References

1. Chen, J.C. Heat Transfer. In *Handbook of Fluidization and Fluid-Particle Systems*, 1st ed.; Yang, W.-C., Ed.; CRC Press: Boca Raton, FL, USA, 2003; pp. 257–286. [CrossRef]
2. Andeen, B.R.; Glicksman, L.R. Heat transfer to horizontal tubes in shallow fluidized beds. In Proceedings of the ASME-AIChE Heat Transfer Conference, St. Louis, MO, USA, 9–11 August 1976; Paper 76-HT-67. American Institute of Chemical Engineers: New York, NY, USA, 1976.
3. Bansal, R.K. Heat Transfer Studies from Single Cylinder and Tube Bundle in Fluidized Bed. Ph.D. Thesis, Georgia Institute of Technology, Atlanta, GA, USA, 1978.
4. Grewal, N.S. A generalized correlation for heat transfer between a gas—Solid fluidized bed of small particles and an immersed staggered array of horizontal tubes. *Powder Technol.* **1981**, *30*, 145–154. [CrossRef]
5. Molerus, O.; Burschka, A.; Dietz, S. Particle migration at solid surfaces and heat transfer in bubbling fluidized beds—II. Prediction of heat transfer in bubbling fluidized beds. *Chem. Eng. Sci.* **1995**, *50*, 879–885. [CrossRef]
6. Mickley, H.S.; Fairbanks, D.F. Mechanism of heat transfer to fluidized beds. *AIChE J.* **1955**, *1*, 374–384. [CrossRef]
7. Martin, H. Heat Transfer in Fluidized Beds. In *VDI Heat Atlas*, 2nd ed.; Stephan, P., Kabelac, S., Kind, M., Martin, H., Mewes, D., Schaber, K., Eds.; Springer: Berlin/Heidelberg, Germany, 2010; pp. 1301–1310. [CrossRef]
8. Kunii, D.; Levenspiel, O. Fluidization and Mapping of Regimes. In *Fluidization Engineering*, 2nd ed.; Kunii, D., Levenspiel, O., Eds.; Butterworth-Heinemann: Boston, MA, USA, 1991; pp. 61–94. [CrossRef]
9. Natale, F.D.; Bareschino, P. Heat transfer and void fraction profiles around a horizontal cylinder immersed in a bubbling fluidised bed. *Int. J. Heat Mass Transf.* **2010**, *53*, 3525–3532. [CrossRef]
10. Kim, S.W.; Ahn, J.Y. Heat transfer and bubble characteristics in a fluidized bed with immersed horizontal tube bundle. *Int. J. Heat Mass Transf.* **2003**, *46*, 399–409. [CrossRef]
11. Pisters, K.; Prakash, A. Investigations of axial and radial variations of heat transfer coefficient in bubbling fluidized bed with fast response probe. *Powder Technol.* **2011**, *207*, 224–231. [CrossRef]
12. Schwaiger, K.B. Development of a Novel Particle Reactor/Heat-Exchanger Technology for Thermal Energy Storages. Ph.D. Thesis, TU Wien, Vienna, Austria, 2017.
13. Hämmerle, M. Auslegung und Konstruktion einer 200[kW]th-sandTES Pilotanlage. Master's Thesis, TU Wien, Vienna, Austria, 2013.
14. Steiner, P.; Schwaiger, K.; Walter, H.; Haider, M. Active Fluidized Bed Technology used for Thermal Energy Storage. In Proceedings of the ASME 2016 10th International Conference on Energy Sustainability, Charlotte, NC, USA, 26–30 June 2016. [CrossRef]
15. Kong, W.; Wang, B.; Baeyens, J.; Li, S.; Ke, H.; Tan, T.; Zhang, H. Solids mixing in a shallow cross-flow bubbling fluidized bed. *Chem. Eng. Sci.* **2018**, *187*, 213–222. [CrossRef]
16. Pécora, A.A.B.; Parise, M.R. Heat transfer coefficient in a shallow fluidized bed heat exchanger with a continuous flow of solid particles. *J. Braz. Soc. Mech. Sci.* **2006**, *28*, 253–258. [CrossRef]

17. Kunii, D.; Levenspiel, O. Heat Transfer between Fluidized Beds and Surfaces. In *Fluidization Engineering*, 2nd ed.; Kunii, D., Levenspiel, O., Eds.; Butterworth-Heinemann: Boston, MA, USA, 1991; pp. 313–336. [CrossRef]
18. Schmidt, K.G. Heat Transfer to Finned Tubes. In *VDI Heat Atlas*, 2nd ed.; Stephan, P., Kabelac, S., Kind, M., Martin, H., Mewes, D., Schaber, K., Eds.; Springer: Berlin/Heidelberg, Germany, 2010; pp. 1273–1277. [CrossRef]
19. Geldart, D. Types of Gas Fluidization. *Powder Technol.* **1973**, *7*, 285–292. [CrossRef]
20. Zabrodsky, S.S.; Antonishin, N.V.; Parnas, A.L. On fluidized bed-to-surface heat transfer. *Can. J. Chem. Eng.* **1976**, *54*, 52–58. [CrossRef]
21. Gelperin, N.I.; Einstein, V.G. Heat Transfer in Fluidized Beds. In *Fluidization*; Davidson, J.F., Harrison, D., Eds.; Academic Press: London, UK, 1971; pp. 471–540. [CrossRef]
22. Bellgardt, D.; Werther, J. A novel method for the investigation of particle mixing in gas-solid systems. *Powder Technol.* **1986**, *48*, 173–180. [CrossRef]